Morph & Slerp

Shape description for 3D printing of concrete

SHAJAY BHOOSHAN
ETH Zurich, Institute of Technology in Architecture, Block Research Group, Stefano-Franscini-Platz, HIB E 45, 8093 Zurich, Switzerland

TOM VAN MELE
ETH Zurich, Institute of Technology in Architecture, Block Research Group

PHILIPPE BLOCK
ETH Zurich, Institute of Technology in Architecture, Block Research Group

ABSTRACT

Synthesis of shapes that are guaranteed to be physically produced by Robotic 3D printing of concrete, needs research attention. This is necessitated by the rapid development of the hardware, commercial availability of and interest in concrete printing. Further the need is amplified by the lack of easy-to-implement-and-use shape-design tools. Together, they provide the context of the proposed work.

A necessary feature for geometries to be 'printable' is that each consecutive layer onto which material is deposited should change gradually such that it has sufficient overlap with the preceding layer (spatial coherence of print paths). The computational handling of these aspects have been introduced by Bhooshan et al. 2018 including the use of a time evolving scalar-field to represent the shape to be designed – the so-called Function Representation (FRep). This paper significantly extends the previous work by (a) fully parametrising the shape description for 3D printing of concrete by decomposing the shape as a combination of shape interpolation (Morph) and affine interpolation (Slerp), and (b) replacing the linear, cross-fading interpolation scheme resulting in physically problematic artefacts with a scheme that produces smooth, spatially coherent outcomes.

An easy-to-implement software application has been prototyped. It couples the shape description with a guiding heuristic to design topologically complex, physically plausible shapes with relative ease. The coupling significantly reduces the effort and expertise needed to produce shapes that are printable whilst also providing intuitive, visual feedback to designers. This is particularly useful in the current context where computer simulation of the stability of the layers during printing is actively being developed, experimental in nature and still computationally expensive. The presented approach does not, however, automatically guarantee printable outputs. The shape description and outputs may, nonetheless, be readily used as good candidates for further optimisation to guarantee print readiness.

SCF '20, November 05, 06, 2020, Virtual Event, USA

ACM ISBN 978-1-4503-8170-3/20/11…$15.00
https://doi.org/10.1145/3424630.3425413

CCS CONCEPTS

• **Applied computing** → Arts and humanities; Architecture (buildings); Computer-aided design; Operations research; Computer-aided manufacturing.

KEYWORDS

3D printing, Robotic concrete printing, Optimal Transport, Displacement Interpolation, Function Representation, shape-design, pitched-brick vaulting

ACM Reference Format:
SHAJAY BHOOSHAN, TOM VAN MELE, and PHILIPPE BLOCK. 2020. Morph & Slerp: Shape description for 3D printing of concrete. In *Symposium on Computational Fabrication (SCF '20), November 05, 06, 2020, Virtual Event, USA.* ACM, New York, NY, USA, 10 pages. https://doi.org/10.1145/3424630.3425413

1 MASONRY, 3D PRINTING AND SCALAR-FIELD INTERPOLATIONS

Robotic 3D printing of shapes in concrete proceeds by depositing layer-by-layer wet concrete that hardens over time, yielding the physical artefact. This is analogous to formwork-free masonry construction. Bhooshan et al. 2018 articulate this analogy particularly in terms of methods of geometry creation, equilibrium analyses and construction sequencing (in stable sections). Furthermore, the work also established the need to explore more suitable shape-design methods given the rapid evolution of concrete-printing hardware and material technologies. Lastly, it also addressed the benefits and the computational handling of explicitly representing and enabling designer manipulation of the printing trajectories along which the robot deposits material – the so-called print paths.

This 'forward design' paradigm is novel in its use for fabrication-process-aware shape representation. It contrasts with the currently ubiquitous 'inverse design' method of 'slicing' process-agnostic 3D shapes, usually represented using Boundary Representation (BRep) schemes, into 2D print layers (Figure 1 a,b). Furthermore, the slicing is typically done by intersecting the input shape with parallel cutting planes. The inverse paradigm can additionally include optimisation routines to modify the input shape to meet several optimality criteria including guarantees to be printable. This is occasionally used in shape-design for desktop-scale, plastic printing [Cacace et al. 2017]. The inverse paradigm, as applied to concrete printing, requires significant domain expertise in both shape creation and concrete printing, apart from routinely leading to difficult-to-solve problems such as the lack of spatial coherence between consecutive print layers (Figure 1). Lack of spatial coherence is also a proxy for

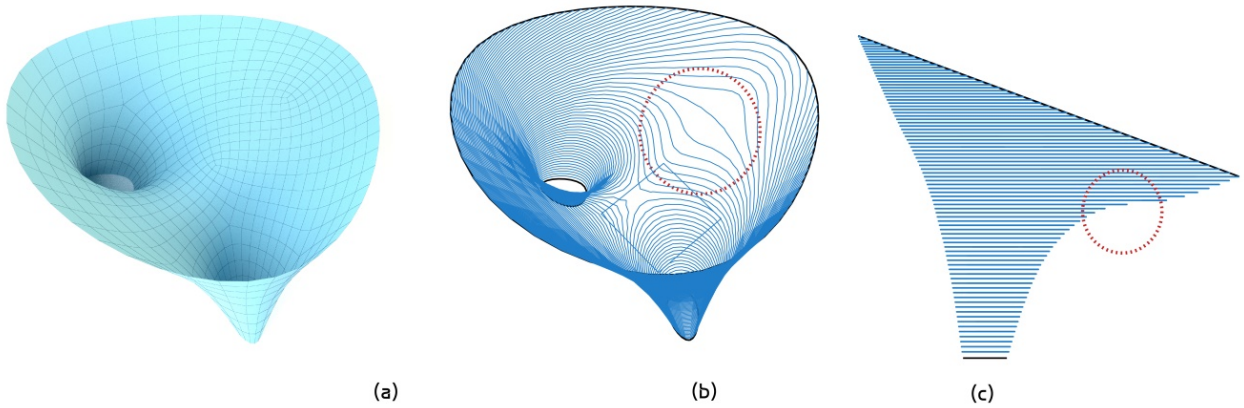

Figure 1: Inverse paradigm: A user-provided mesh (a), typically modelled agnostic to printing constraints, is 'sliced' to derive print paths (b) by intersecting horizontal cutting planes with the input mesh. . The dashed red circle highlights the problematic parts for printing due to a lack of spatial coherence (b) causing infeasible, unsupported overhangs between subsequent layers(c).

other problems such as extreme inclination and cantilever of the layers in cross section (Figure 1 b,c).

In contrast, the proposed work follows a process-aware, forward-design paradigm. It focusses on automatically synthesising print layers with spatial coherence, based on user-provided boundary conditions of start and end print paths and print planes (Figures 2, 3, 4). Importantly, the proposed shape-design method significantly reduces domain expertise needed to create topologically complex, nearly-print-ready shapes. It also provides visual feedback with regard to constraints of concrete printing due to the explicit representation of the print paths and the implementation of a guidance heuristic. Lastly, it is easy to implement and extend. The outputs of the proposed method of shape-design, though not automatically guaranteed to be printable, serve as a good starting point to guide towards printable outcomes due to in-built spatial coherence of the generated print paths.

Specifically, Bhooshan et al. 2018 exemplify the advantages of using an evolving scalar-field representation scheme – the so-called Function Representation (FRep) and its zero contours to represent the print paths and thus the 3D shape. Furthermore, they also highlight the limitations of linear, cross-fading interpolation of scalar-fields, such as abrupt transitions and lack of spatial coherence between consecutive print layers. This paper significantly extends the previous work by adding shape-design aspects that are simultaneously designer-friendly and improve printability of the designed shapes. In particular, it focusses on developing appropriate scalar-field interpolation schemes, adapting ideas from the field of Optimal Mass Transport.

1.1 Key contributions

The motivation of the research is to address the lacunae in interactive, designer-friendly shape-design tools that provide practical and didactic understanding of the physical viability of shapes for concrete 3D printing and other layered construction techniques such as corbelling and pitched-brick vaulting [Bhooshan et al. 2018]. The work presented here focuses on parametric shape description and providing guidance with respect to printability, i.e. that the printed layers will not collapse during printing or the wet phase of concrete. Currently, there is a lack of such tools.

The key innovation is fully parameterising shape description for 3D printing by decomposing the shape as a combination of shape interpolations between start and end cross sections (Morph) and affine interpolation between corresponding start and end planes (Slerp). The principal contribution is thus a task-appropriate shape-interpolation scheme adapted from the Displacement Interpolation [Bonneel et al. 2011] and Optimal Mass Transport [Papadakis 2015]. We also couple the shape description with a guiding heuristic to design novel, topologically complex, physically plausible shapes without requiring extensive domain expertise in shape-design for 3D printing. All the outcomes were produced using a proof-of-concept, stand-alone shape-design application that couples tightly with downstream applications that process shapes for robotic printing.

2 PRIOR WORK

As mentioned previously, Bhooshan et al. 2018 introduced two key ideas – analogy of concrete printing to masonry design and construction and the use of FRep. The masonry analogy is particularly important because the currently ubiquitous parallel-slicing paradigm in 3D printing share s its features and limitations with brick corbelling where by each layer of material partially overhangs the previous to produce shapes. The proposed work aims to extend the analogy to pitched-brick masonry which employs evolving non-parallel courses, and thus the range of viable shapes. Resonance of some of these aspects can be found in recent work [Carneau et al. 2020]. Specifically in the context of shape-design, however, the following are the important precedent research.

2.1 Shape-design for Pitch brick masonry

Wendland 2007 studied the design of historic masonry structures, particularly the so-called pitched-brick vaults that did not use supportive formwork during the laying of the bricks. Specifically, he showed that they are compound structures made up of simpler primitives of geometry, which in turn consist of bricks laid along self-supporting arched courses. Both the laying of bricks and lack of supportive formwork is strikingly similar to 3D printing along print paths. Thus, a primitive of shape-design for 3D printing could similarly be composed of i) two cross-sectional curves with their respective planes of orientation and ii) interpolated, in-between curve shapes and their respective interpolated planes. Thus, the work by Wendland is an important precedent to the Morph & Slerp formulation introduced in this paper. It is worth noting that in Wendland's reconstruction, and generally, in masonry structures, the two curves are usually of the same topology, and that interpolation is thus trivial.

2.2 Optimal Mass transport

Optimal Mass Transport has its historic roots in a problem formulated and addressed by Gaspard Monge – the famous Earthmovers problem of minimising the amount of work needed to move earth from its sources to sinks where they are needed. In image processing, optimal transport is the geodesic between two images. Papadakis 2015 provides a comprehensive treatment of the topic.

Optimal Transport has found many uses in recent times, particularly in image processing [Papadakis et al. 2014], geometry processing (Solomon et al. 2015) and machine learning [Peyré and Cuturi 2019]. To the best of our knowledge, its use in 3D printing and the design of printable shapes has not been explored. Both the displacement and geodesic perspectives are relevant to our task and work – moving a source FRep to a target FRep in a spatially coherent fashion.

2.3 Spatially coherent scalar-field interpolation using mass transport

Mass Transport is optimal if it preserves total mass to be transported from one location to another and minimises total work needed to do so. In the context of shape-design using FRep, however, the optimality is not strictly necessary and instead another property is useful: the spatial coherence between subsequent temporal states of the transport. Therefore, Optimal Transport is often called Displacement Interpolation. There are two main methods to compute Displacement Interpolation: i) a Eulerian formulation that is based on mass-preserving computational fluid dynamics [Papadakis et al. 2014] (Figure 2) and ii) a discrete Lagrangian formulation that moves mass-carrying points from source to target locations (Figure 3).

Bonneel et al. 2011 show the earliest use of the Lagrangian Mass Transport to compute the interpolation between two given bidirectional reflectance distribution function (BRDF) maps – a common intermediate image object needed in rendering pipelines to create computationally generated images. In that context, they note the advantages of using the Lagrangian model including computational speed and parameter control. Our work and paper particularly adapts the ideas and some of the code from this important precedent work [Bonneel et al. 2011; Bonneel 2018; "Network Simplex." 2009].

3 MORPH AND SLERP SHAPE DESCRIPTION

Our two part, FRep-based description of the shape to be 3D printed consists of i) start and end scalar-fields and their respective orientation planes and ii) interpolated in-between scalar-fields (Morph) and their respective interpolated planes (Slerp).

3.1 Morph: Shape Interpolation

As mentioned previously, Bonneel et al. 2011 developed a Lagrangian formulation to compute the interpolation between two BRDF images – in other words, an interpolation between two continuous functions. Their pipeline consists of i) decomposing the two continuous functions into their respective radial basis functions (RBFs) by adequately sampling the functions, ii) computing the Optimal Transport between all paired RBFs represented as mass points with a radius of influence (Figure 4 a,b) iii) advecting the mass points along the geodesic paths between paired mass points (Figure 4 c), and, finally, iv) reconstructing the interpolated function (the interpolated BRDF image) from the advected RBFs.

In our current framework to shape-design for 3D printing using FRep, we adapted the RBF-based Lagrangian optimal-transport framework as follows:

a) Start with two user-defined RBFs thus omitting the first and last step (Figure 4 a,b). The RBFs are represented as mass points with a radius of influence. The length of straight-line or curved paths between each pair of mass points represents the cost of moving a unit mass between the centres. In terms of shape-design, they represent the paths along which the shape will evolve (Figure 4 d, Figure 6 (a,b), Figure 11 c).
b) Retain the mass-transport and advection steps to compute the interpolated RBFs. We use the zero contours of the interpolated, time-evolving RBFs to represent consecutive print layers. Thus, the stack of n zero-contours represents the overall shape of the 3D object 5 b). The number n provides intuitive user control over the 'resolution' or thickness of the print layers. These curves are transformed to their respective interpolated planes (5 c). The resulting 3D shape (Figure 5 d) is thus a combination of shape and plane interpolation between given end states.
c) Add parameters to control the rate of displacement of the individual mass points of the source RBF, as they move from source locations to computed target locations. This allows the calibration of rate of interpolation such that two consecutive zero contours have sufficient overlap i.e. have spatial coherence (See section 4).
d) Add control curve handles to define the paths from sources to sinks. This allows for more user control of the resulting 3D shape (Figure 6). In particular, they allow for control over how the generated shape looks in the top-view or cross-sectional view (Figure 6 b,c). We use procedurally generate these control curves by 'walking' between source and target mass points of a user-provided graph (Figure 6 a) and computing the so-called Dijkstra shortest paths (Figure 6 b);

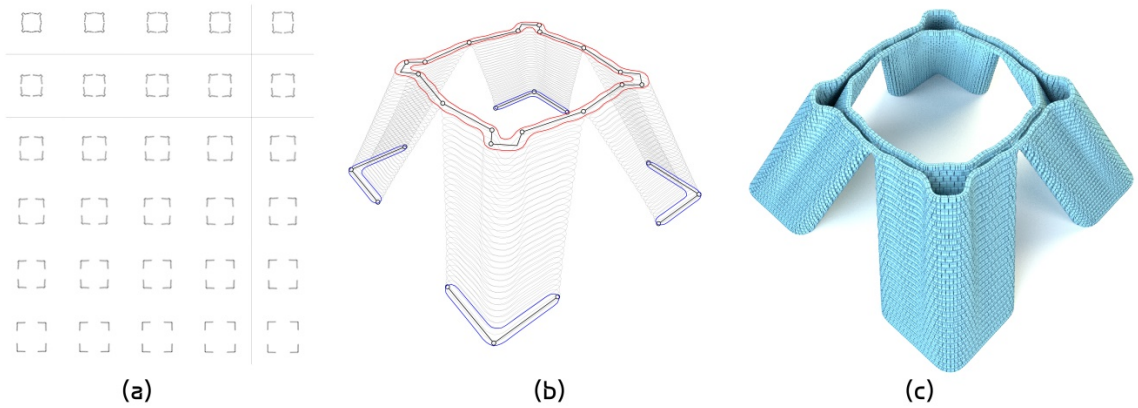

Figure 2: Fluid-dynamics-based, Eulerian optimal transport: (a) The fluid-dynamics formulation of Optimal Transport[Papadakis et al. 2014] and corresponding C++ code [Bonneel 2013] was used to produce this interpolation sequence of morphing top-left image to bottom-right image; (b) corresponding zero contours with start (red), end profile(blue) and interpolated zero-contours(grey), (c) resulting 3D shape obtained by stacking the consecutive zero contours.

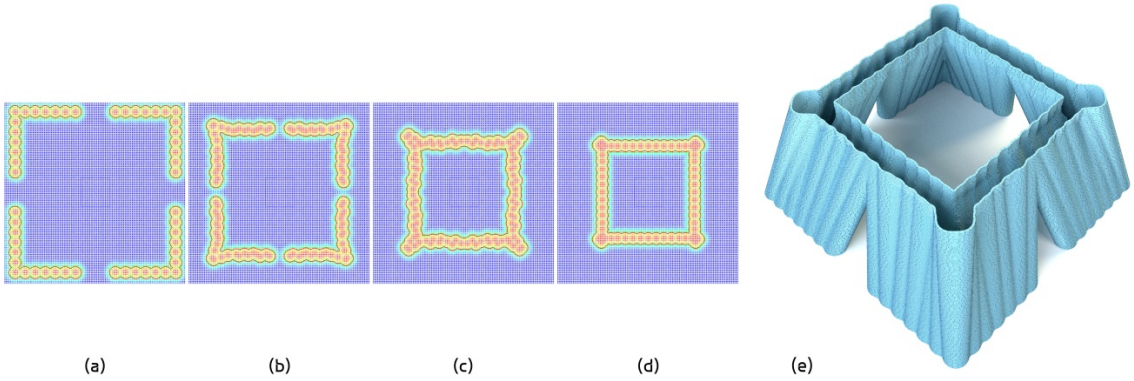

Figure 3: Radial Basis Function (RBF) based, Lagragian optimal transport: (a,d) Source and target RBF-based scalar-field; (b,c) intermediate, interpolated RBF and scalar-field state; The Displacement Interpolation algorithm and corresponding C++ code was adapted to produce this interpolation sequence [Bonneel et al. 2011; Bonneel 2018;"Network Simplex." 2009] (e) resultant 3D shape achieved by stacking the consecutive zero contours.

3.2 Slerp: Plane Interpolation

The second part of our shape description for 3D printing consists of interpolating the start and end orientation planes. The zero-contour curves of the interpolated scalar-fields from the previous step are transformed to these interpolated planes. In effect, these interpolated planes represent the planes of the print paths and material deposition. This is analogous to the titled planes of brick courses in pitched-brick masonry. We can use any affine interpolation scheme for this purpose. We describe two well-established schemes used in computer animation: curved motion paths and the associated Frenet-Serret moving frames (Figure 7 b-left) and Spherical Interpolation (Figure 7 b-right)

3.3 Motion paths and Frenet-Serret frames

A user-friendly method to generate the interpolated planes between user-provided start and end planes would be to extract in-between planes from a user-provided Bezier curve connecting the centers of the two planes. The Bezier curve can be drawn such that the start and end tangents of the curve are aligned with the normal of the start and end planes. In practice, the start and end planes are extracted from the drawn curve. The so-called Frenet-Serret moving frame consisting of the tangent, normal and binormal at each point along the curve can provide the in-between orientation planes.

In particular, we can use a curve based on the path of the resultant of the flow of forces in the final structure, which will improve the structural alignment of the print paths normal to the expected force transmission across the layers (Figure 7 c). This is structurally beneficial once the 3D print hardens.

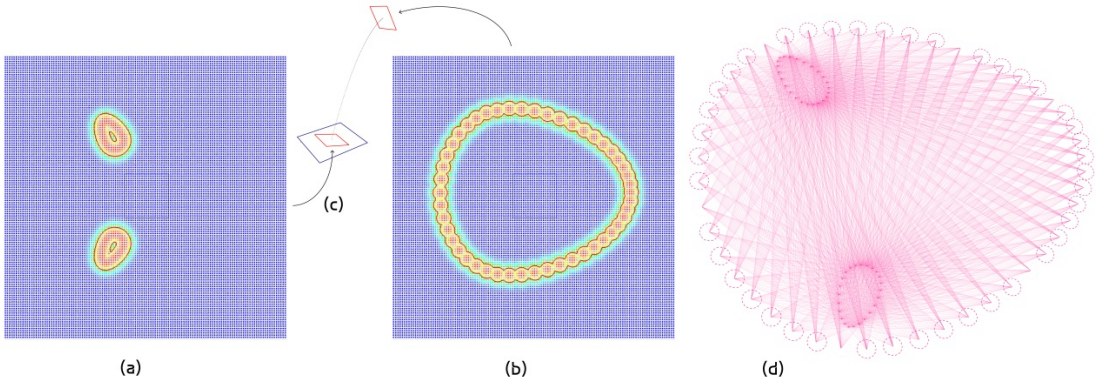

Figure 4: Planar Inputs: (a,b) Starting and end scalar-fields and corresponding zero-contours (red) produced by respective Radial Basis Functions (RBFs) (dashed). (c) User-provided start and end print planes (red) and optionally a curve connecting them (d) In-plane Euclidean paths between centres of all pairs of RBFs of starting and end scalar-fields. Alternatively, segmented paths may be generated from a graph connecting the centers (Figure 6).

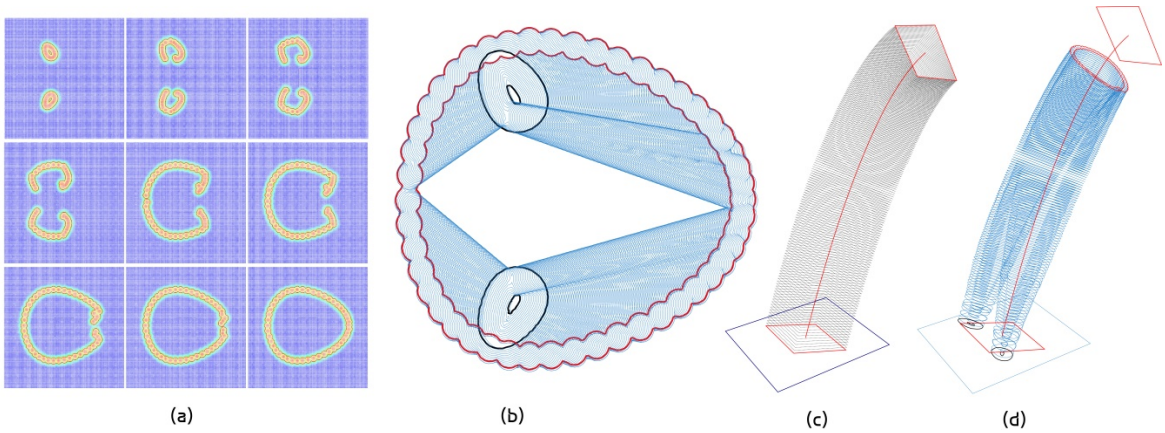

Figure 5: Morph & Slerp: (a,b) Morph operation – blending two topological circles in the starting scalar-field to one in the end, (c,d) Slerp operation. (a) Displacement interpolation between start and end scalar-fields. (b) Zero-contours extracted in-plane and in-place, from various intermediate states of the evolving scalar-field shown in (a). (c) Moving frames (black) extracted from a curve connecting the start and end planes (red). (d) Resulting 3D shape achieved by transforming each in-plane curve (b) unto respective planes in (c).

3.4 Spherical Linear Interpolation

A robust, numerically stable, compact and well-established way to represent orientation in 3D space is using quaternions. A natural interpolation that extends from this choice, is the so-called Spherical Linear Interpolation scheme [Shoemake 1985]. This single-parameter interpolation is useful to produce an initial set of interpolated planes for user manipulation and also for procedural optimisation.

3.5 Affine transformation and spatial coherence

One of the consequences and an easy visual check of the spatial coherence of the zero-contours obtained from the Morph operation (Section 3.1) is the smooth gradation of the size of the bounding boxes of each of the contours (Figure 8a). Given such smoothness, the contours can individually be scaled to fit a unit square without loss of spatial coherence (Figure 8). This feature is useful when designing tubular shapes and to constrain the external boundary of the shape within a unit square (Figure 8 d,e and Figure 11).

4 PARAMETER CHOICE

Given the two-part, Morph & Slerp shape description, the intrinsic parameters that control the overall shape are:

a) RBFs defining start and end scalar-fields and corresponding centres / mass points;
b) individual rates of displacement of centres of source RBF towards target RBFs; and

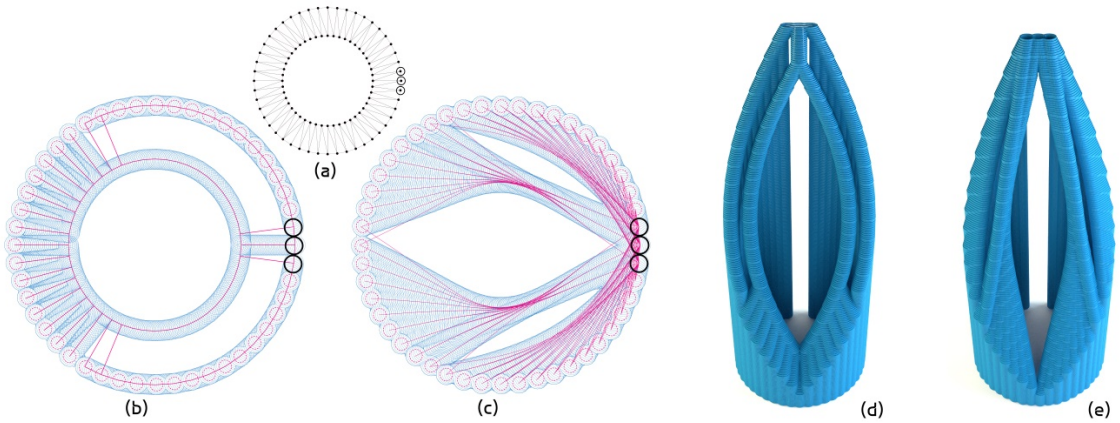

Figure 6: Displacement trajectories: (a) User-provided graph connecting centers of source RBF (black circles) and sink RBF (black dots); (b) a family of segmented curve handles generated by walking between source (black circles) and target mass points (pink dashed circles) marked on graph in (a) and computing the so-called Dijkstra paths; (c) smoothed version of the family of curves shown in (b). It can be noted that the zero-contours of the shape (blue) evolve along the control curves in both (b) and (c); (d,e) resulting 3D shapes corresponding to (b) and (c) respectively, with the smooth family(c) producing more gentle curvature and inclination in the print layers, hence more amenable to printing with wet concrete. Thus control handles similar to (c) is recommended.

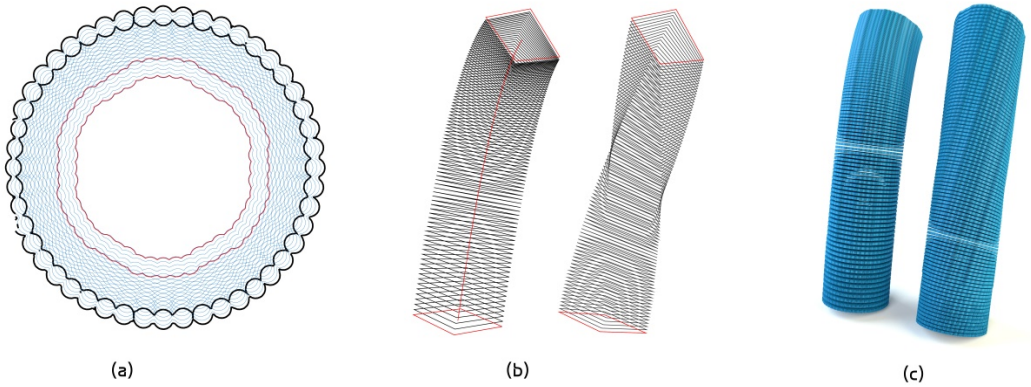

Figure 7: Plane interpolation: (a) Intermediate profile curves (blue) obtained by interpolating between start (red) and end (black) profiles using the Morph operation (Section 3.1); (b-left) Frenet-Serret moving frames extracted from a curve (red) and (b-right) spherical linear interpolation of frames between start and end frames (red); (c) resulting 3D shapes obtained by transforming (a) unto each family of planes (b-left and b-right) and subsequently thickening the curves.

c) orientation quaternions of each individual plane – if these quaternions come from Slerp, every interpolated plane will produce a control parameter; If a Bezier curve controls them, the location of the control points of the curve become the parameters.

In a typical example, there can be 50 centres and thus 50 displacement rates, and if the stack is of 100 layers say, we can have a 100-segment curve. Thus, finding a printable shape is the equivalent of finding 150 parameters. These parameters can be found either by heuristically guided user-manipulation or through procedural optimisation. In this work, we focus on the former.

4.1 Guiding heuristic

3D printing in concrete has two important material and process aspects to be considered: i) the stability of the printed layers during printing, and ii) failure of the material upon non-axial loading after the print is hardened. The former is the primary concern for the shape-design process. Currently, there are no available tools to compute the buckling stability of the print layers, with the exception of recent work [Ghent and Concre3DLab 2019; Wu 2020]. We use the corbelled-masonry analogy [Bhooshan et al. 2018] and provide a simple, geometric heuristic as guidance – the extent of overlap between print paths lying on consecutive print planes (i.e. consecutive print layers) with each path having a fixed, lateral in-plane width

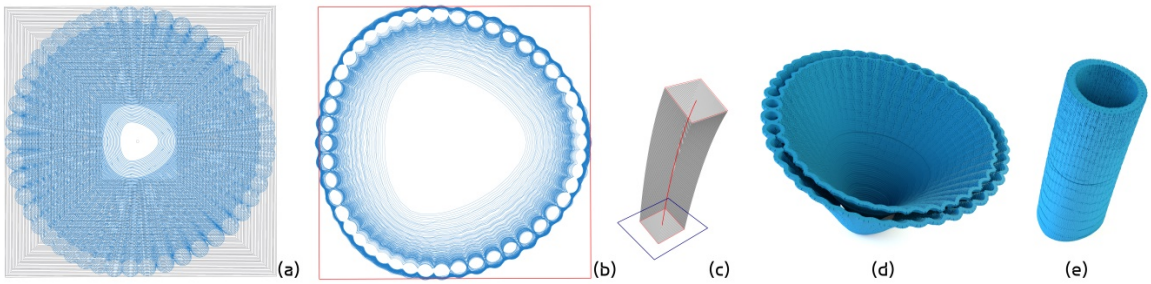

Figure 8: Affine Transformation: (a) Zero-contours of interpolated scalar-field (blue) obtained from the Morph operation (Section 3.1). The smooth gradation of bounding boxes of each consecutive zero contour (black squares) is a consequence of the spatial coherence of the zero-contours. (b) Each of the zero-contours of (a) individually scaled to fit a unit square. (c) Interpolated planes using the Slerp operation (Section 3.2); (d) resulting 3D shape obtained by affine transformation of each (a) unto (c). (e) resulting 3D shape obtained by affine transformation of each (b) unto (c).This shows the use-case of scaling all zero-contours to fit within a unit square and generating tubular shapes (see Section 3.5).

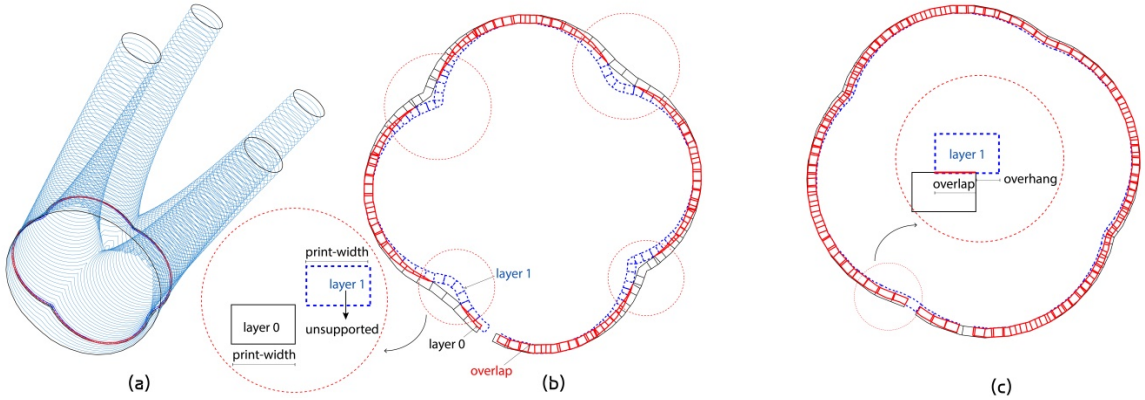

Figure 9: Guiding heuristic: (a) Typical check for spatial coherence between two consecutive print layers; (b) zoom-in of (a) and an example of two consecutive layers exhibiting partial lack of spatial coherence between them (dashed red circles). Layer 1(blue) is to be printed on top of layer 0 (black) and thus needs sufficient overlap interface (red) to be adequately supported. When curves are not fully coherent, layer 1 can become partially or entirely unsupported (inset); (c) zoom-in of (a) and an example of two consecutive layers exhibiting good spatial coherence between themselves and thus adequate overlap (red line in inset) and overhang within bounds.

(so-called print width) relating to the size of the printing nozzle. If a minimum overlap is not met – usually half the print width - it implies that the portion of the print-path is unsupported and thus likely to fall through. A minimum (but not sufficient) criterion for successful completion is that a minimum overlap is consistently met everywhere across each pair of consecutive layers (Figure 9). This heuristic is aligned with visual inspection practices of experienced 3D printing professionals and similar to the well-known corbelled-brick heuristic in the masonry trade where a one-third of the length upper brick can overhang the lower brick – in other words one third of the upper brick can be cantilevered.

The heuristic is easy to compute and thus computationally tractable to be used within an optimisation routine. Importantly, it is also intuitive from a design perspective. Thus, the heuristic can help users to manipulate the shape parameters to improve printability. This heuristic attempts to geometrically capture very many material and mechanical parameters that influence the stability of the layers during printing [Suiker 2018; Wangler et al. 2016]. Thus, the heuristic, whilst not guaranteeing successful printing, does provide significant visual feedback to designers and an easy check for minimum (not sufficient) criterion for a successful print. This is particularly useful in the current context where computer simulation of the stability of the layers during printing is rapidly evolving, but still experimental in nature and computationally expensive.

5 RESULTS

The highly sensitive combination of material and process parameters means that in practice, for all but the simplest extrusions, it is simpler and more reliable to physically validate the shape. This

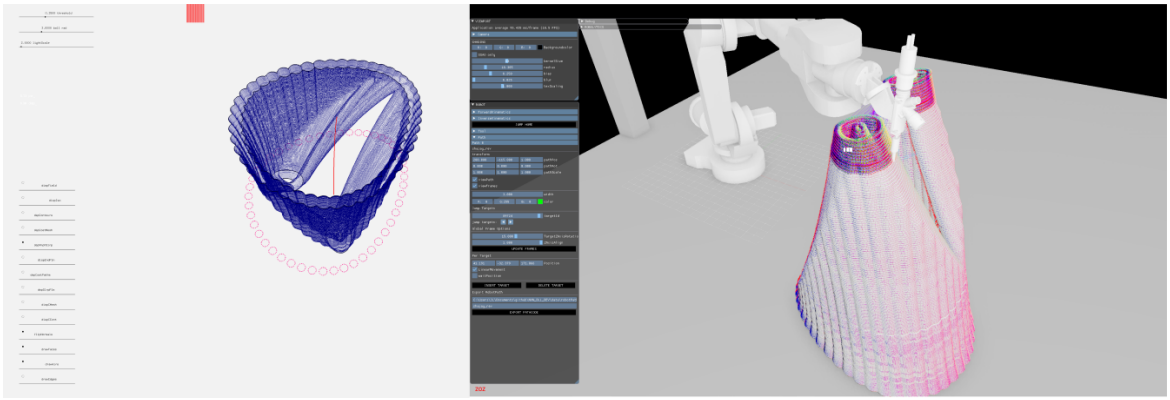

Figure 10: Stand-alone applications: (left) Proof-of-concept, stand-alone computer application to synthesise shapes for robotic 3D printing using the proposed method; (right) application for downstream processing of geometry for manufacturing used (courtesy of Incremental 3D GmbH).

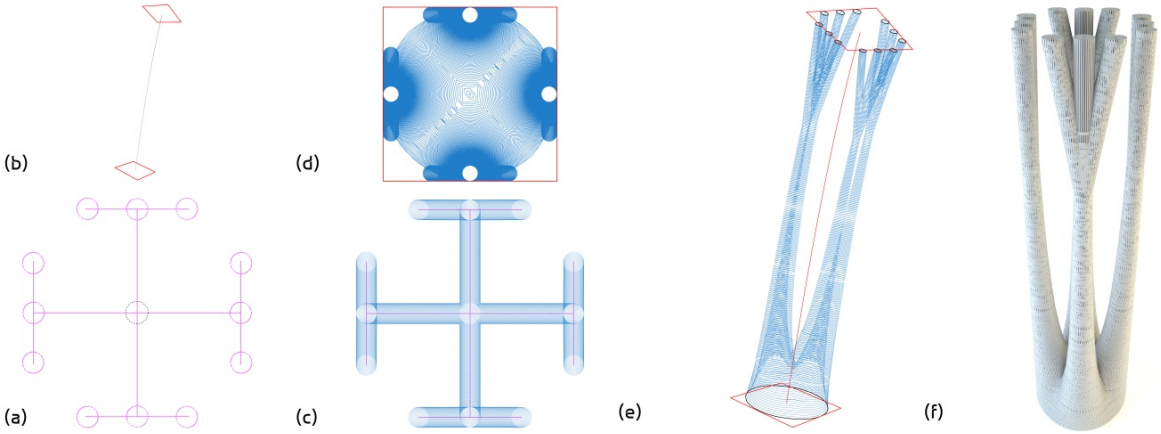

Figure 11: Branching topology and inclined print paths example: The proposed shape description only requires (a) graph with location of start and end mass-points (pink and black dashed circles respectively), and start and end planes (b) to automatically produce spatially coherent, gradually inclined print paths of a topologically complex shape (e) (see Section 3). (c,d) Intermediate zero-contours created from inputs (a,b) (See Section 3.5). It would require considerable expertise in both BRep based shape modelling and 'slicing' to produce (e) using currently ubiquitous methods (see Section 1); (f) 3D shape obtained by thickening the (blue) curves in (e);

requires that the design-to-production pipeline is as streamlined as possible. The proposed shape description is well aligned with the downstream requirements of print paths and print-plane normals for end-effector orientation (Figure 10right). As such, there is nominal downstream processing to turn the generated shape into a physical artefact. Further, two fully encapsulated software applications are sufficient to complete the design-to-production pipeline (Figure 10). The proposed, lightweight shape description enables the two applications to communicate via text-based file formats.

The creation of topologically complex shapes and intricate shape features requires significant domain expertise and experience in the current 'slicing' paradigm (Section 1). This requirement is significantly reduced with the proposed paradigm (Figure 11and Figure 12).

Lastly, the bulbous curvature of the cross-sectional curves (undulating profile) (Figure 12), are a feature of the RBF-based formulation of mass transport used in the research (Section 2.2). Smooth curves are possible with the fluid-dynamics formulation mentioned previously (Figure 13). It can be noted again that the specific optimal transport formulation to be used (Fluid/Eulerian or RBF/Lagragian) does not change the Morph & Slerp shape description or the functioning of the tool.

6 LIMITATIONS AND OUTLOOK

The immediate outlook of the research relates to some of the limitations of the current work and to the yet-to-be explored branches leading from the main thrust of the work so far:

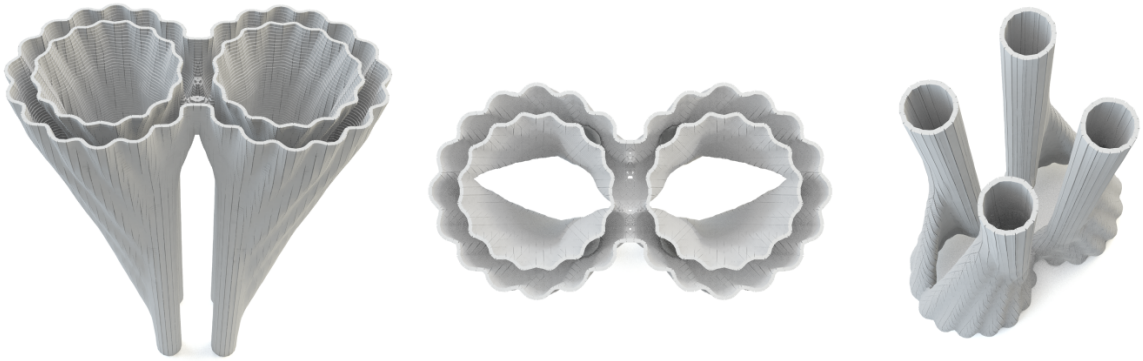

Figure 12: Lagrangian Optimal mass transport example: (L-R) Top-down, top and bottom-up offline rendered views of an example geometry produced using the Morph & Slerp shape description. The displacement interpolation scheme used in this paper makes it easy to create spatially coherent blends between cross sectional curves with different topology such as in this example – four circles of the bottom profile are morphed into two touching circles on the top cross section. The bulbous curves are a feature of the RBF-based formulation (see Section 2.2).

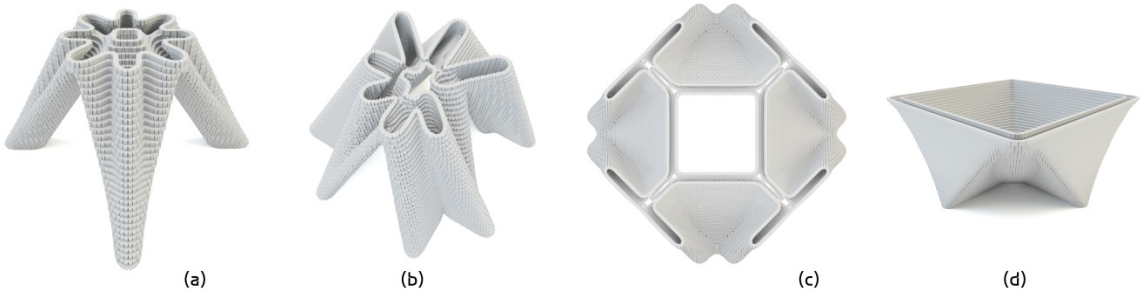

Figure 13: Eulerian Optimal mass transport examples. (a-d) Offline rendered images of example geometries with spatially-coherent blends between pairs of profiles curves, produced with relative ease using the Morph & Slerp shape description; These examples highlight the possibility of having smooth curve profiles if we use the fluid-dynamics-based formulation of optimal transport (see Section 2.2) instead of the bulbous curves that are a feature of the RBF-based formulation used in Figure 12. The M&S shape description can admit either of the two formulations of optimal transport.

- Currently, the input scalar-fields and the interpolated fields are restricted to RBFs. However, we intend to explore the recovery of a continuous function from interpolated RBFs using convolution methods, as noted previously. In addition, we note that if the final step of recovering a continuous function from point samples were required, quick convolution methods can be used [Fuchs 2020]. It can be noted that these bulbous features can be smoothed out using a weighted averaging post-processing step also.
- The proposed shape description can be combined with skeletal graphs to generate compound shapes consisting of multiple coordinated Morph & Slerp parts. This will extend previously explored processing of funicular skeletons for materialisation via 3D printing [Bhooshan et al. 2018].
- Currently, print paths are restricted to planar paths. Physically, non-planar print paths are feasible to a limited extent. The intention is to capture the description of such print paths within the local coordinate frame of the orientation planes.
- We also intend to explore optimal mass transport with relaxed optimality criteria as they will still yield spatially coherent print paths whilst improving the computational speed of the interpolation scheme.
- An interesting future avenue of exploration would be to calibrate the shape description for other layered constructions, particularly pitched-brick vaulting.

7 CONCLUSION

In conclusion, the initial results of the research are promising and suggest several immediate avenues of progress. The proposed shape description method takes a foundational step towards addressing the current lack of shape-design tools that are designer friendly in

the edit-and-observe, didactic sense. The research will benefit from calibration against physical printed results.

The immediate next steps stem from the following features of the proposed shape description:

1. It is intuitive, compatible with visual inspection and reasoning.
2. It provides users with control handles to generate a variety of topologically complex shapes features with simple input.
3. It is lightweight in terms of computational storage, with two RBF-based scalar-fields and two quaternions being sufficient to describe all the print paths of a generated shape, often with complex topology.
4. It is fully parametric; Thus, compatible to collate and compactly organise a large shape library, similar to image libraries.

The last two features in particular may be useful for machine-learning applications that need compact and easy-to-process representations. In particular, shape-to-vector type shape classification applications and applications that optimise process parameters of 3D printing could benefit.

Taken together with the proposed outlook, the proposed Morph & Slerp shape description provides the necessary foundation to build interactive and didactic applications to promote design for both the rapidly evolving robotic 3D printing of concrete and other historic layered construction techniques such as masonry vaulting.

REFERENCES

Bhooshan, Shajay, Tom Van Mele, and Philippe Block. 2018. "Equilibrium-Aware Shape Design for Concrete Printing." In Humanizing Digital Reality, edited by K De Rycke *et al.*, 493–508. Paris: Springer Singapore. https://doi.org/10.1007/978-981-10-6611-5_42.

Bhooshan, Shajay, Johannes Ladinig, Tom Van Mele, and Philippe Block. 2018. "Function Representation for Robotic 3D Printed Concrete." In Robotic Fabrication in Architecture, Art and Design, 98–109. Springer.

Bonneel, Nicolas. 2018. "Fast Network Simplex for Optimal Transport." https://github.com/nbonneel/network_simplex

Bonneel, Nicolas. 2013. "Optimal Transport with Proximal Splitting." https://perso.liris.cnrs.fr/nicolas.bonneel/FastTransport/.

Bonneel, Nicolas, Michiel Van De Panne, Sylvain Paris, and Wolfgang Heidrich. 2011. "Displacement Interpolation Using Lagrangian Mass Transport." In Proceedings of the 2011 SIGGRAPH Asia Conference, 1–12.

Cacace, Simone, Emiliano Cristiani, and Leonardo Rocchi. 2017. "A Level Set Based Method for Fixing Overhangs in 3D Printing." Applied Mathematical Modelling 44: 446–55.

Carneau, Paul, Romain Mesnil, Nicolas Roussel, and Olivier Baverel. 2020. "Additive Manufacturing of Cantilever-From Masonry to Concrete 3D Printing." Automation in Construction 116: 103184.

Fuchs, Mathias. 2020. "Quick Convolution." https://github.com/Mathias-Fuchs/quickconvolution.

Ghent, Concre3DLab. 2019. Numerical Simulation of 3D Concrete Printing. https://www.youtube.com/watch?v=5NVRJTvCJxc.

"Network Simplex." 2009. http://lemon.cs.elte.hu/pub/doc/latest-svn/a00783.html.

Papadakis, Nicolas. 2015. "Optimal Transport for Image Processing."

Papadakis, Nicolas, Gabriel Peyré, and Edouard Oudet. 2014. "Optimal Transport with Proximal Splitting." SIAM Journal on Imaging Sciences 7 (1): 212–38.

Peyré, Gabriel, and Marco Cuturi. 2019. "Computational Optimal Transport." Foundations and Trends®in Machine Learning 11 (5–6): 355–607.

Shoemake, Ken. 1985. "Animating Rotation with Quaternion Curves." In Proceedings of the 12th Annual Conference on Computer Graphics and Interactive Techniques, 245–54.

Suiker, A S J. 2018. "Mechanical Performance of Wall Structures in 3D Printing Processes: Theory, Design Tools and Experiments." International Journal of Mechanical Sciences 137: 145–70.

Wangler, Timothy, Ena Lloret, Lex Reiter, Norman Hack, Fabio Gramazio, Matthias Kohler, Mathias Bernhard, Benjamin Dillenburger, Jonas Buchli, and Nicolas Roussel. 2016. "Digital Concrete: Opportunities and Challenges." RILEM Technical Letters 1: 67–75.

Wendland, David. 2007. "Traditional Vault Construction without Formwork: Masonry Pattern and Vault Shape in the Historical Technical Literature and in Experimental Studies." International Journal of Architectural Heritage 1 (4): 311–65.

Wu, Shaun. 2020. "Buckling Simulation in Karamba3D." 2020. https://www.karamba3d.com/projects/buckling-simulation-for-3d-printing-in-fresh-concrete/.